RSC Advances

ROYAL SOCIETY OF CHEMISTRY

www.rsc.org/advances

Synthesis and characterization of SiO_2/polyaniline/Ag core-shell particles and studies of their electrical and hemolytic properties: Multifunctional core-shell particles

Dhaneswar Das,[a] Parag Choudhury,[a] Lakhyajyoti Bortahkur,[a] Bhaskarjyoti Gogoi,[b] Alak Kumar Buragohain,[b] Swapan Kumar Dolui[a,*]

[a]Department of Chemical Sciences, India

[b]Department of Molecular Biology and Biotechnology, India.

*Corresponding author: dolui@tezu.ernet.in

Department of Chemical Sciences, Tezpur University, Tezpur 784028, Assam, India.

Tel.: +91 9957198489.

Abstract

Three layers conducting core-shell nanocomposites particles composed of SiO_2/Polyaniline (PAni)/Ag were prepared in the presence of silicon dioxide (SiO_2) in aqueous solution containing sodium dodecyl benzenesulfonate (SDBS) as a surfactant. SiO_2 nanoparticles were coated by PAni, which results in the formation of core-shell nanocomposites. Silver nanoparticles synthesized by citrate reduction method. Ag nanoparticles could be electrostatically attracted on the surface of SiO_2/PAni nanocomposites, leading to formation of SiO_2/PAni/Ag nanocomposites with core-shell structure. The products were characterized by Fourier transform infrared (FT–IR) spectroscopy, X–ray diffraction (XRD), scanning electron microscopy (SEM), transmission electron microscopy (TEM), current–voltage (I–V) analysis and cyclic voltammetry (CV). The resultant nanocomposites have good biological property.

Key words: Ag nanoparticles, SiO_2 nanoparticles, Nanocomposites, conducting polymer, Electrical Conductivity.

Introduction

In recent years conducting polymers with multifunctional core-shell structures have received considerable interest because of their conductivity, magneto-rheological response, electronic properties, mechanical properties and easy processing. [1-5] Conducting polymers such as poly (p-phenylene sulfide), polyaniline (PAni), polyacetylene, polythiophene, poly (p-phenylene vinylene), polypyrrole (PPy) etc, always have been the center of attraction due to their conducting nature and found to be suitable for sensors, actuators, light emitting diodes, capacitors, battery electrodes etc. [6-8] Amongst conducting polymers, PAni shows some great promises due to its excellent environmental and chemical stability. [9-10] PAni and its composites have been extensively applied for their electrorheological fluids.[11-12] The core-shell structure is particularly interesting because the core can be imitative to make the particle such as fluorescent or magnetic, independent of the shell properties. The core-shell structures between silica sphere and conducting polymer have attracted attention. [13-14] A thin layer of conducting PAni reduces the cost and enhances surface area which is favorable for application in catalysis, controlled delivery and in photographic industry. The uses of silica as core have some advantages like high colloidal stability and easily controllable particle size. [15]

Silica nanoparticles are used in enormous products ranging from cosmetic to construction materials. It has a potential application in the drug delivery, biosensors. [16-17] The use of nanoparticles with core-shell or multilayer morphology allows one to obtain complex compositional and structural patterns in the ultimate nano composite material. Generally silica NPs are in colloidal form or agglomerated dry powder. However, simply PAni undergoes rapid degradation in performance upon repetitive cycles of charging and discharging due to its swelling and shrinkage. [18-20] In order to improve these limitations, the incorporation of silica with PAni has been proved to reinforce the stability.

Silver nanoparticles have potential used in health care delivery due to its antimicrobial and wound healing properties. [21] Silver salts or metallic silver have been used to prevent bacterial infections associated with medical devices, such as wound dressings, catheters, and orthopedic and cardiovascular implants, with different degrees of clinical efficacy. Due to its high surface to volume ratios silver nanoparticles have high reactivity and hence it provides a new platform for use in both consumer and biomedical applications. [21-22]

Now-a-days, three layer core-shell nanocomposites have been gaining much attention. Three-layered core-shell structures with Au-modified PPy-coated Ag nanocomposites through the mixing of Au colloidal solution with PPy/Ag were reported. Au/PPy/Ag nanocomposites were immobilized on the surface of a glassy carbon electrode and utilized to construct a dopamine biosensor. The synthesized biosensor could detect dopamine at its low concentration in the presence of 5000 times concentration of ascorbic acid at neutral environment. [6] A tri layer core shell nanostructure where silica as core with Fe_3O_4 and Au as inner, outer shells, respectively were prepared. These core-shell magnetic nanoparticles have excellent DNA binding properties as well as magnetic properties. [23] Synthesis of silica-PAni core-shell nanoparticles by in-situ polymerization was reported. The synthesized silica–PAni core-shell nanoparticles showed pH-responsive redox reversibility and relatively high electrical conductivity. [24] Fe_3O_4/PPy/Au core-shell nanoparticles with excellent electrocatalytic properties with good magnetism were reported. The resultant nanocomposites easily controlled by an external magnetic field but also have the good conductivity and excellent electrochemical and catalytic properties of PPy and Au nanoparticles. Furthermore, the nanocomposites showed excellent electrocatalytic activities to bio-species such as ascorbic acid. [25] Three layer core-shell nanocomposites with NiO/PPy/Ag as the core, inner shell and outer shell was also reported. The synthesized nanocomposites provide

good electrical conductivity with the increase of NiO nanoparticles content. The core-shell nanocomposites showed an enhanced bactericidal effect and hence it can be used in water purification technology. [26] Highly conductive and crystalline PAni onto silica nanoparticles with core-shell morphology were prepared by using self-stabilized dispersion polymerization method. [27] The conductivity of the core-shell nanoparticles depends upon the diameter of the particles. As the diameter of the silica-PAni core-shell nanoparticles decreased from 130 to 18 nm, the electrical conductivity of the core-shell nanoparticles was found to be increased from 16.4 to 25.6 Scm^{-1}.

In this work, a facile approach has been developed for the fabrication of SiO_2/PAni/Ag core-shell nanoparticles. The SiO_2 nanoparticles were synthesized by hydrolysis of TEOS followed by thermal decomposition and it is used as a core for the synthesis of core-shell nanoparticles. PAni shell was formed over the surface of SiO_2 nanoparticles by *in-situ* polymerization of positively charged anilinium ions on the negatively charged of the silica nanoparticle through electrostatic forces. Finally SiO_2/PAni/Ag nanocomposites were formed by the electrostatic interaction between the Ag nanoparticles and PAni chain and thereby we obtain three layer SiO_2/PAni/Ag core-shell structure. The synthesized nanocomposites showed good electrical conductivity as well as the hemolytic property.

Experimental Section

Materials

Tetra ethoxy silane, aniline, sodium dodecylbezenesulfonate (SDBS) were purchased from Sigma Aldrich. $AgNO_3$, HCl, $(NH_4)_2.S_2O_8$, tri-sodium citrate dehydrates, acetonitrile, NH_4OH, KCl were purchased from Merk, India. All the chemicals were of analytical grade. Deionized,

distilled water and purified ethanol were used as dispersion medium for all the chemical preparation as well as for washing.

Method

Preparation of Silicon dioxide (SiO_2) nanoparticles

SiO_2 nanoparticles were prepared by the hydrolysis of tetra ethoxy silane (TEOS). [28] In a typical synthesis process, TEOS (6 mL) and ethanol (40 mL) were mixed under low frequency ultrasound. Hydrolysis of TEOS is performed by the addition of about 1 mL of distilled water. About 2.55 mL of NH_4OH solution was added to the reaction medium and the mixture was sonicated for 2 h. This results the gelation in the reaction medium. The gel was centrifuged and properly washed with a mixture of ethanol and water to remove the unwanted impurities. The samples were freeze dried for about 12 h. The collected sample was heated in the muffle furnace at about 600°C for 2 h. Then it was allowed to cool to room temperature and collect the resultant mass.

Preparation of silver (Ag) nanoparticles

A colloidal stable dispersion of Ag nanoparticles was synthesized by citrate reduction method. [29-30] 50 mL 0.001 M $AgNO_3$ solution in distilled water was taken in a conical flask and heating up it with constant stirring to boiling. 5 mL of 1% tri-sodium citrate solution was added into it. The solution was turned into light yellow in color. This color results the formation of Ag nanoparticles. Stirring was continued until the solution became cool down to room temperature.

Preparation of SiO_2/PAni core-shell nano composites

PAni was prepared by using chemical oxidation of aniline monomer in the acidic solution of a non-anionic surfactant. SiO_2/PAni core-shell nano composites were prepared by in-situ polymerization technique with slight modification, where SiO_2 is the core and the PAni is the

shell of the composites. [31] Freshly prepared silica nanoparticles were dispersed in an aqueous solution of SDS (0.05 g, 30 mL water). The mixture was sonicated for about 30 min. After that, it was transferred into a solution composed of 4.50 g of aniline, 7.50 mL of 1 M HCl, 150 mL of water at room temperature and stirred it for 1 h. 1.15 g of $(NH_4)_2.S_2O_8$ (APS) was dissolved in 50 mL of distilled water. The APS solution was transferred to the reaction mixture and the reaction was allowed to proceed for 24 h at room temperature without disturbing. The resultant products were separated by filtration followed by washing with distilled water and then methanol for several times. The products were dried at 60°C in an oven for 24 h. Different core-shell particles of SiO_2/PAni were prepared by changing the amounts of SiO_2 nanoparticles keeping other ingredients constant.

Preparation of SiO_2/PAni/Ag three layered nanocomposites

Ag nanoparticles were adsorbed on PAni coated SiO_2 nanocomposites by electrostatic interaction. SiO_2/PAni nanocomposites were added into the Ag nanoparticles colloidal solution at a concentration of 2.50 mg/mL under stirring condition and the stirring was continued for 48 h. Ag nanoparticles attracted on the surface of the SiO_2/PAni nanocomposites, which leads to the formation of SiO_2/PAni/Ag core-shell nanocomposites. The light yellow color of the Ag nano colloidal solution turned colorless with the increasing time of mixing. Finally, the resultant product was separated from the solution and dried under vacuum.

Characterization

Fourier transforms infrared (FTIR) spectroscopy

The FTIR spectrum of the composites was recorded in Nicolet Impact-410 IR spectrometer in KBr medium at room temperature in the range of 400-4000 cm^{-1}.

Scanning Electron Microscopy (SEM)

SEM micrographs of the core-shell particles were taken with a Jeol-JSM-6390L V scanning electron microscope. Composite samples were sputter coated with platinum thickness of 200A°.

Transmission Electron Microscopy (TEM)

The size and morphologies of the products were observed with a JEOL JEM 2100 transmission electron microscope at an acceleration voltage of 200 kV. In the TEM measurement, the samples were prepared by dropping highly diluted composites on the carbon coated copper grid and dried in a vacuum oven at room temperature.

Thermo gravimetric analysis (TGA)

Thermo gravimetric analysis of the products was studied in a Shimadzu TA50 thermal analyzer. The heating was done under nitrogen atmosphere at a heating rate of 5^{o}C /min in the range of 25-700^{o}C.

Electrical conductivity

Pellets of composite samples were made by using a compression molding machine with hydraulic pressure. High pressure was applied to the sample to get hard round shaped pellet (1.5 cm diameter, 2 mm breadth) which will be used in measuring conductivity.

The electrical conductivity of SiO_2/PAni and SiO_2/PAni/ Ag composites were measured by using four probe techniques. I-V characteristic was studied by Keithley 2400 sourcemeter at the room temperature in the frequency range 102-106 Hz. The voltage was applied to measure the current passing through the sample.

Cyclic Voltammetry (CV) measurement was performed on an electrochemical work station Sycopel AEW2-10 with an Ag/AgCl reference electrode, a platinum wire as a counter electrode and PAni coated SiO_2 core-shell composite and PAni-Ag coated SiO_2 core-shell films (1, 3, 5, 7 and 10% SiO_2 with respect to the monomer) on ITO coated glass as working electrode. The

electrochemical characteristics of the composite sample were investigated by cyclic voltametric scanning at a scan rate of 50 mVs^{-1}. A solution of 0.1 M KCl prepared in 10 ml acetonitrile was used as supporting electrolyte.

Method for Haemolysis Assay

According to the method described by Zhu et al., the haemolytic assay was performed with little modification to check the lysis of the RBC membrane by the SiO_2/PAni/Ag nanoparticles. [31] For that the blood was collected in a tube containing 4% sodium citrate and centrifuged at 3000 rpm at 4°C for 15 min. The supernatant was aspirated and the erythrocytes were washed with phosphate saline buffer (PBS, pH 7.4) for three times. After washing, 5% packed erythrocytes were gently resuspended with PBS. Different concentrations of the nanoparticles (0.5 mg/mL, 1 mg/mL, 2.5 mg/mL, 5 mg/mL, 10 mg/mL, and 20 mg/mL) were mixed gently with the haematocrit in the ratio of 95: 5 (V: V). 1% Triton X100 was used as the positive control as it can lyse the RBC cells and PBS as the negative control. The mixtures were incubated for 1 h at 37°C. After the termination of the incubation period, the cells were placed in an ice bath for 1 min and then centrifuged at 3000 rpm for 10 min at 4°C. The measures of hemolysis were observed by taking absorbance 540 nm.

Result and Discussions

FT-IR analysis

The FT-IR spectrum of SiO_2 nanoparticle, Ag nanoparticles, SiO_2/PAni-Ag nanocomposites are shown in the Fig. 1. (a), (b), (c). In the FT-IR analysis of SiO_2 nanoparticles, [Fig. 1(a)], there are three absorption bands are seen in the region of 1500-450 cm^{-1}. A characteristic absorption band is observed at 475 cm^{-1}, due to racking mode of the Si-O-Si group. An absorption band at 806 cm^{-1} is due to the symmetric stretching of Si-O-Si bond. A sharp band at 1112 cm^{-1} corresponds

to asymmetric stretching of Si-O-Si bond. These absorption bands indicate the formation of SiO_2 nanoparticles. The absorption bands at 1169, 1268 and 1637 cm^{-1} indicates the formation of Ag nanoparticles [Fig. 1(b)]. The 1308 cm^{-1} band is assigned to the C-N stretch of a secondary aromatic amine whereas, in the region of 1010-1170 cm^{-1}, the aromatic C-H in-plane bending modes are usually observed [Fig. 1(c)]. Out-of-plane deformations of C-H on 1, 4-disubstituted rings are located in the region of 800-880 cm^{-1}. The region 900-700 cm^{-1} corresponds to the aromatic ring and out-of-plane deformation vibrations.

Thermal stability

To investigate the thermal stability of PAni, SiO_2/PAni, SiO_2/PAni-Ag core-shell nanocomposites, thermo-gravimetric analysis were performed [Fig. 2]. From the analysis it is seen that every sample undergoes two stage weight losses. The first weight loss at about 40-100^oC is due to loss of residual moisture from the polymer matrix. PAni is stable upto 250°C. But core-shell composites particles degradation occurs at 300°C. Core-shell composite particles degrade at higher temperature. The residual weight for SiO_2/PAni (5%), SiO_2-PAni (7%) are found to be 48.41 and 54.05 respectively at 600°C. The residual weight for SiO_2/PAni/Ag (5%), SiO_2-PAni/Ag (7%) are found to be 61.94 and 62.10 respectively at 600°C. TG-analysis reveals that there is an improvement in the thermal stability of the PAni as well as SiO_2/PAni-Ag composites due to the incorporation of SiO_2 and Ag nanoparticles into the polymer matrixes.

X-ray diffraction (XRD) analysis

XRD analysis was performed to investigate the crystalline or amorphous nature of the nanoparticles and the nanocomposites. XRD patterns of Ag nanoparticles, SiO_2 nanoparticles, PAni and SiO_2/PAni-Ag core-shell nanocomposites are shown in the [Fig. 3(a), (b), (c) (d)]. XRD peak for Ag nanoparticles are observed at 2θ angle 38° (111), 44° (200) and 64° (220) [Fig.

3(a)]. Pure SiO_2 nanoparticles give a XRD peak at 2θ angle 21.2° [Fig. 3(b)]. These characteristic peaks indicate the formation of SiO_2 nanoparticles. Pure PAni is amorphous is nature and hence it gives a broad XRD peak with 2θ angle in between 19.45 to 30.40 [Fig. 3(c)]. The XRD peaks at 38° (111), 44° (200) and 64° (220) for SiO_2/PAni-Ag nanocomposites indicates the successful incorporation of Ag into the SiO_2/PAni core-shell nanocomposites [Fig. 3(d)].

Scanning Electron Microscope (SEM) analysis

To determine the surface morphology of the nanoparticles and the nanocomposites, SEM was performed. Fig. 4(a) shows the SEM image of the SiO_2 nanoparticles. The SiO_2 nanoparticles were found to be the nearly uniform shape and the particles are found in the range from 30-40 nm. SEM image of PAni [Fig. 4(b)] display the tubular structure with outer diameter 55-60 nm. SEM image [Fig. 4(c)] of SiO_2/PAni shows that the outer diameter of the SiO_2/PAni (size 80-90 nm) is greater than that of pure SiO_2 nanoparticle (55-60 nm). This information proves the successful incorporation of PAni onto SiO_2 nanoparticles. The dotted spot in the SEM image of SiO_2/PAni is may be due to the presence of SiO_2 nanoparticles in the composites. The SEM image of the SiO_2/PAni/Ag is given in the [Fig. 4(d)]. The diameter of this composite is more than that of the SiO_2/PAni. This implies the successful attachment of the Ag nanoparticles on the surface of the SiO_2/PAni.

Energy Dispersive X-ray (EDX) analysis

To identify the presence of the elements, the core-shell nanocomposites were characterized by EDX-analysis. [Fig. 5] represented EDX image of SiO_2, SiO_2/PAni and SiO_2/PAni-Ag core-shell nanocomposites. Presence of only Si and O peak in the Fig. 5(a) indicates the formation of pure SiO_2 nanoparticles. The presence of Si and O peak in the EDX graph [Fig. 5(b)] indicates the

presence of SiO_2 in SiO_2/PAni nanocomposites. Presence of C and N peaks indicates the successful formation of PAni over SiO_2 nanoparticles. The existence of Ag peak [Fig. 5(c)] indicated the attachment of Ag nanoparticles on SiO_2/PAni surface.

Transmission Electron Microscope (TEM) analysis:

Fig. 6 represents the TEM images of SiO_2 nanoparticles, Ag nanoparticles, SiO_2-PAni core-shell nanocomposites, SiO_2/PAni-Ag core-shell nanocomposites. In the Fig. 6(a), the synthesized SiO_2 nanoparticles are found to be spherical and the average size of the nanoparticles is found to be about 40 nm. Fig. 6(b) represents the TEM image of Ag nanoparticles and the average particles size of the particles is found to be 10-15 nm. TEM image [Fig. 6(c)] of SiO_2-PAni nanocomposites, shows core-shell structure. It is seen that dark spots with diameter about 40-45 nm coated by light shaded shell structure. This result confirms the successful coating of PAni on SiO_2 nanoparticles and resulting the formation of SiO_2-PAni nanocomposites with core-shell morphology. The doted spots on the surface of SiO_2/PAni-Ag nanocomposites [Fig. 6(d)] indicate the successful attachment of Ag nanoparticles on the surface of SiO_2/PAni nanocomposites.

Electrical behavior

Current-Voltage (I-V) relationship

The current-voltage relationships for the SiO_2/PAni-Ag composites with different Ag content are performed to study the conducting behavior of the composites and it is shown in the Fig. 7. Fig. 7 denotes the I-V relationship of PAni as well as the core-shell nanocomposites with various compositions of Ag at room temperature. From the I-V analysis of the core-shell nanocomposites exhibit a non-ohmic behavior as V/I is not proportional and it indicates that the core-shell nanocomposites particles behave as a Schottky junction. This exponentially behavior of the I-V

curves can be explained with the help of conducting mechanism of PAni. In case of conducting polymers such as PAni, charge conduction is carried by the formation of polarons (electrons) and bipolarons (holes) in addition to free charge carriers. Whenever the applied voltage increases, the formation of polarons and the bipolarons increases quickly which results the rapid increase in current in comparison to the applied voltage and hence results an exponential I-V curve. With increase of Ag nanoparticles content in the PAni matrix, the exponential behaviour of the I-V curves gradually decreases. This is because, interactions takes place between Ag nanoparticles and the PAni. Hence with the increase of Ag nanoparticles content into the shell phase, the potential difference (in Volt) increases exponentially with the applied current (in mA). Hence, it may be concluded that the synthesized core-shell nanocomposites are of semiconducting nature.

Electrochemical property

To investigate the redox properties of the nanocomposites, Cyclic-Voltammetry (CV) analysis was conducted by varying SiO_2 nanoparticles in the composites. Fig. 8 represents the CV graphs of SiO_2/PAni nanocomposites with different SiO_2 nanoparticles content (0, 1, 3, 5, 7 and 10% respectively). The shapes of the CV graphs of the nanocomposites were found to be different from the PAni. The electrochemical band-gap of the nanocomposites was calculated by using the following formulae:

$$\text{HOMO} = -[\varphi^{ox}_{onset} + 4.71]\ (\text{eV}) \quad (1)$$

$$\text{LUMO} = -[\varphi^{red}_{onset} + 4.71]\ (\text{eV}) \quad (2)$$

$$E^{g}_{ec} = [\varphi^{ox}_{onset} - \varphi^{red}_{onset}]\ (\text{eV}) \quad (3)$$

where the units φ^{ox}_{onset} (onset oxidation potential) and φ^{red}_{onset} (onset reduction potential) are V vs Ag/AgCl. The electrochemical band gap of PAni was found to be higher than that of SiO_2/PAni [Table-1]. The electrochemical band gaps of SiO_2/PAni are found to decrease from

2.01 eV to 1.32 eV with the increasing amount of SiO_2 in the core-shell nanocomposites. The peak currents for the composite were higher compared with those for PAni. The decrease of electrochemical band gapes were also observed [Fig. 9] after the deposition of Ag nanoparticles in the surface of PAni shell and it was listed in the Table-2. This enhancement in current may be attributed to the special nanostructure of this composite. The change in electronic band structure manifested as new mid-gap state being created and theirby decreasing of electrochemical band gap of the composites.

Charge capacity:

To investigate the charge capacity of the nanocomposites, CV analysis was performed upto 100 repeated cycles. Fig. 10 represents the CV graph of the nanocomposites up to 100th cycle. The area under the CV peaks could be integrated to produce charge capacity of the nanocomposites, which gives information about the electro activity of the nanocomposites. From the analysis it clearly revealed that cathodic peaks and anodic peaks were approximately symmetrical above each other with least separation. The charge capacity of the core-shell nanocomposites did not get reduced even after the repeated cycles. From this analysis we can concluded that the final material can be used in rechargeable battery material.

DC Electrical conductivity

The DC electrical conductivities of the synthesized core-shell nanocomposites with varying the amount of SiO_2 nanoparticles content in the core phase were measured at the room temperature (25°C) and it tabulated in the Table 3. From the conductivity measurements it is seen that the conductivity value of the SiO_2/PAni, SiO_2/PAni-Ag core-shell nanocomposites are found to be higher than that of the pure PAni. It is gradually increases with the increasing the amount of SiO_2 nanoparticles in the core. The DC-electrical conductivity value of the core-shell

nanocomposites vary in the range from 0.15 X 10^{-3} Scm^{-1} to 5.88 X 10^{-3} Scm^{-1}. The conductivity value of the core-shell nanocomposites changes rapidly with the deposition of Ag nanoparticles. This increase in conductivity of the core-shell nanocomposites may be due to the increased compactness of the composite material as the growing polymer chains are supported on the SiO_2 nanoparticles. Thus, on incorporation of SiO_2 particles into the polymer, which restricts the twisting of the polymer backbone away from its planarity and hence the polymer chains become more ordered. This results the linking between the polymer chains is increasingly improved and at the same time it provides a higher DC electrical conductivity of the PAni/SiO_2 core-shell nanocomposites compared with pure PAni.

Hemolytic assay:

The lysis of the RBC membrane was investigated by RBC haemolytic assay to observe hemolytic of the Ag. The percentage of the haemolytic activity was observed very less in comparison to the positive control [Fig. 11]. The inhibition percentage of hemolysis is equal to the negative control when the cells treated with the nanoparticles of concentration upto 5 mg/mL. But it showed a little hemolysis activity when the cells treated with 10 mg/mL and more than that. When the cells treated with the different amounts of the nanoparticles, the absorbance at 540 nm is less in the nanoparticle treated cells compared to the cells treated with Triton X-100. According to the literature, the absorptivity at 540 nm is observed due to the presence of hemiglobincyanide. [32] Since the absorbance is less in nanoparticles treated cells, it implies that the lysis of the RBC is less and equal to the negative control due to which the hemoglobin molecules could not come out from the cells. But in case of Triton X-100 treated cells, though it can rupture the cell membrane, the hemoglobin molecules can come out from the cells due to

which the absorbance is observed more. Hence it can be considered that the nanoparticles have the hemolytic property upto optimum level.

Conclusions

At summary, we have successfully synthesized the multicomponent SiO_2/PAni/Ag nanocomposites with core-shell morphology, where SiO_2 as the core which is coated with conducting polymer, PAni as the inner shell and Ag nanoparticles are attached on the surface of PAni. UV, FTIR, XRD, SEM and TEM analysis confirmed the formation of SiO_2 and Ag nanoparticles. FT-IR and XRD analysis confirmed the formation of PAni, SiO_2/PAni and SiO_2/PAni/Ag. From the TG-analysis, we have concluded that the nanocomposites have potentially stable to heat and it is increases with the incorporation of SiO_2 nanoparticles into the polymer matrixes. From the CV analysis it is seen that with the incorporation of SiO_2 the electrical property enhances. The nanocomposites are stable under cyclic redox potential upto 100 cycles and hence it can be used in re-chargeable battery material. From the hemolytic analysis it can be confirmed that the final core-shell nanocomposites, i.e. SiO_2/PAni/Ag is shows the hemolytic property upto an optimum level. This simple approach could provide an opportunity to design unique core-shell nanostructures with different functionality.

Acknowledgements:

The authors would like to acknowledge the help and support of Tezpur University authority. The first author would also like to acknowledge receipt of the Rajiv Gandhi National fellowship from UGC, India [Sanction Number: F. 16-1884(SC)/2010 (SA-III), Dated: 18.07.2011]

References

1. Q. Yu, M. Shi, Y. Cheng, M. Wang and H. Chen, *Nanotechnology,* 2008, **19**, 265702-265707.

2. S. Xuan, Y. J. Wang, K. C. Leung and K. Shu, *J. Phys. Chem. C,* 2008, **112**, 18804-18809.
3. F. F. Fang, Y. D. Liu, H. J. Choi, and Y. Seo, ACS Appl. Mater. Interfaces 2011, **3**, 3487-3495.
4. F. F. Fang, Y. D. Liu, I. S. Lee, and H. J. Choi, *RSC Advances,* 2011, **1**, 1026-1032.
5. W. Yan, X. Feng, X. Chen, X. Li and J. Zhu, *Bioelectrochem.,* 2008, **72**, 21-27.
6. F. Hui, B. Li, P. He, J. Hu and Y. Fang, *Electrochem. Commun.,* 2009, **11,** 639-642
7. L. Pan, H. Qiu, C. Dou, Yun Li, L. Pu, J. Xu and Yi Shi, *Int. J. Mol. Sci.,* 2010, **11**, 2636-2657
8. D. Li, J. Huang, and R. B. Kaner, *Acc. Chem. Res.,* 2009, **42**, 135-145,
9. H. Xia and Q. Wang, *Chem. Mater.,* 2002, **14**, 2158-2165.
10. K. Zhang, H. Chen, X. Chen, Z. Chen, Z. Cui and B. Yang, *Macromol. Mater. Eng.,* 2003, **288**, 380-385.
11. J. Lu, and X. Zhao, *J. Mater. Chem.***,** 2002, **12**, 2603-2605.
12. P. Hiamtup, A. Sirivat, and A. M. Jamieson, *J. Colloid Interface Sci*., **295,** (2006) 270-278.
13. G. Li, G. Liu, E. T. Kang, K. G. Neoh, and X. Yang, *Langmuir*, 2008, **24**, 9050-9055
14. F. Iskandar, Mikrajuddin, and K. Okuyama, *Nano Lett.,* 2002, **2**, 389-392.
15. Y. S. Jeong, W. Oh, S. Kim and J. Jang, *Biomater,* 2011, **32**, 7217-7225.
16. Q. He and J. Shi, *J. Mater. Chem.,* 2011, **21**, 5845-5855.
17. D. N. Upadhyay, S. Bharathi, V. Yegnaraman, and G. P. Rao, *Sol. Energy Mater. Sol. Cells*, 1995, 37 307-314.

18. S. Xiong, P. Jia, K. Y. Mya, J. Ma, F. Boey, and X. Lu, *Electrochim. Acta*, 2008, **53,** 3523-3530.

19. T. Tuken, B. Yazıcı and M. Erbil, *Appl. Surf. Sci.,* 2006, **252,** 2311-2318.

20. K. Chaloupka, Y. Malam, and A. M. Seifalian, *Trends Biotechnol.,* 2010, **28,** 580-588.

21. S. W. P. Wijnhoven, W. J. G. M. Peijnenburg, C. A. Herberts, W. I. Hagens, A. G. Oomen, E. H. W. Heugens, B. Roszek, J. Bisschops, I. Gosens, and V. D. Meent, *Nanotoxicology*, 2009, **3**, 109-138.

22. S. I. Stoeva, F. Huo, J. S. Lee and C. A. Mirkin, *J. Am. Chem. Soc.,* 2005, **127**, 15362-15363.

23. J. Jang, J. Ha and B. Lim, *Chem. Commun.*, 2006, 1622-1624.

24. H. Zhang, X. Zhong, J. Xu, and H. Chen, *Langmuir,* 2008, **24**, 13748-13752.

25. D. Das, B. C. Nath, P. Phukon, B. J. Saikia, I. R. Kamrupi and S. K. Dolui, *Mater. Chem. Phys.,* 2013, 142, 61-69.

26. M. Kim, S. Cho, J. Song, S. Son, and J. Jang, *Appl. Mater. Interfaces*, 2012, **4**, 4603-4609.

27. W. Stober, A. Fink and J. Bohn, *J. Coll. Int. Sci*. 1968, **26**, 62-69.

28. A. Sileikaite, I. Prosycevas, J. Puiso, A. Juraitis and A. Goubiene, *Mater. Sci.* 2006, **12,** 287-291.

29. L. Rivas, S. S. Cortes, J. V. G. Ramos and G. Morcillo, *Langmuir,* 2001, **17**, 574-581.

30. Q. Y. Zhu, R. R. Holt, S. A. Lazarus, T. J. Orozco and A. L. Keen, *Exp. Biol. Med.,* 2002, **227**, 321-329,.

31. B. M. Lee, J. E. Kim, F. F. Fang, H. J. Choi, and J. Feller, *Macromol. Chem. Phys.* 2011, ***212***, 2300-2307.

389 32. W. G. Zijlstra and A. Buursma, *Comp. Biochem. Physiol.* 1997, **118**, 743-749.

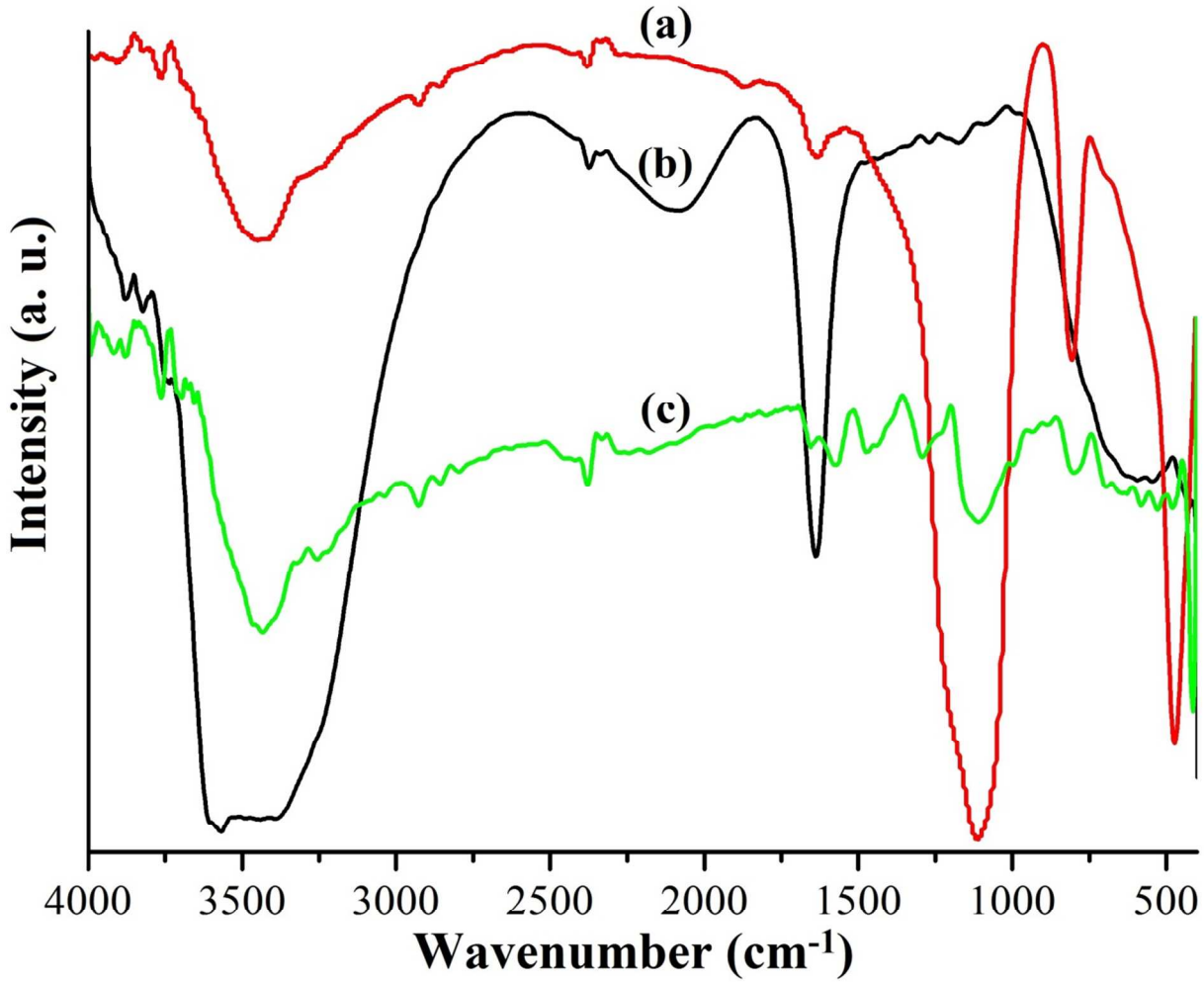

390

391 **Fig. 1** The FT-IR spectrum of (a) SiO_2 nanoparticle, (b) Ag nanoparticles, (c) SiO_2/PAni-

392 Ag nanocomposites.

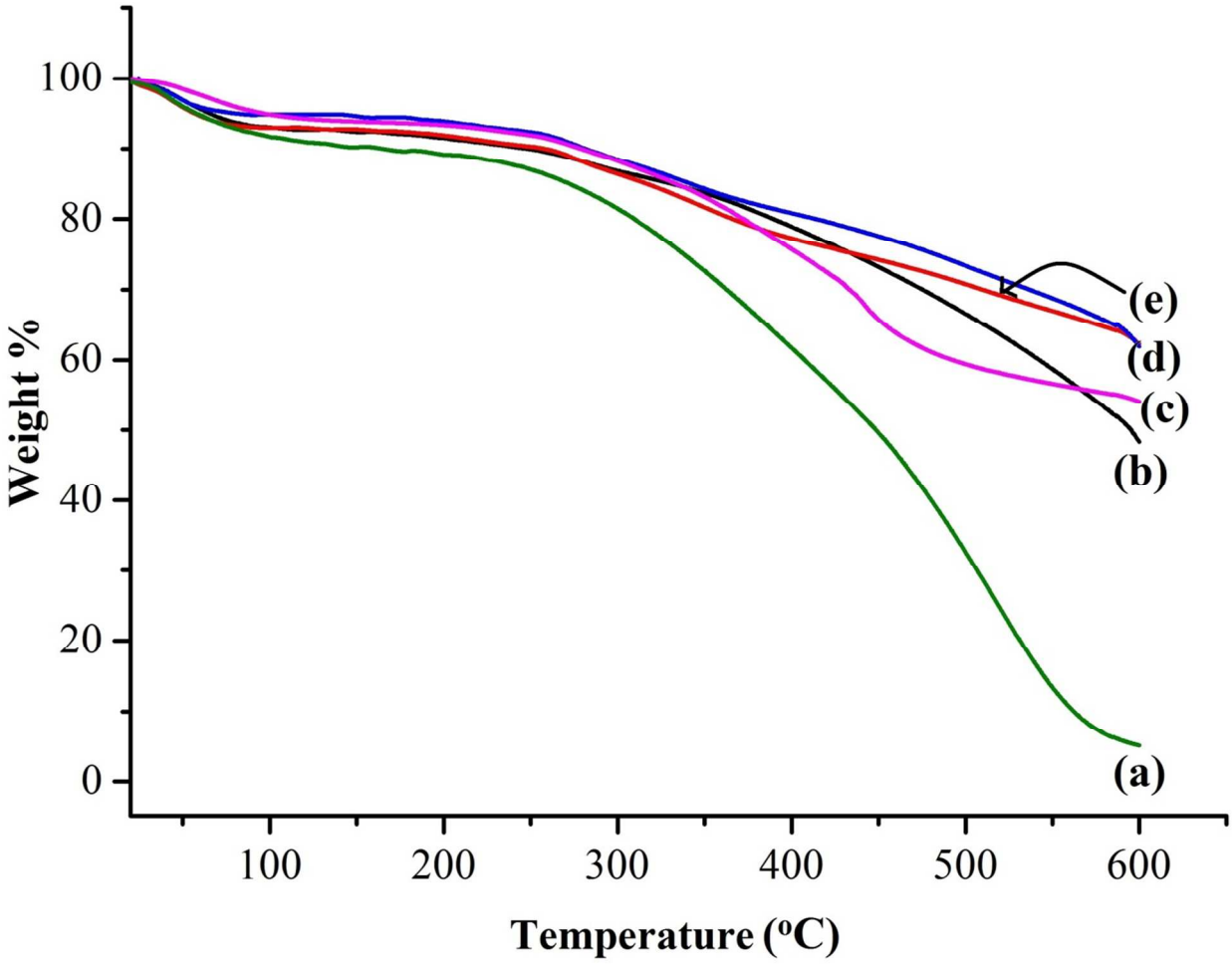

Fig. 2 TGA analysis of (a) PAni, (b) SiO_2/PAni (5%), (c) SiO_2/PAni (7%), (d) SiO_2/PAni-Ag (5%), (e) SiO_2/PAni-Ag (7%).

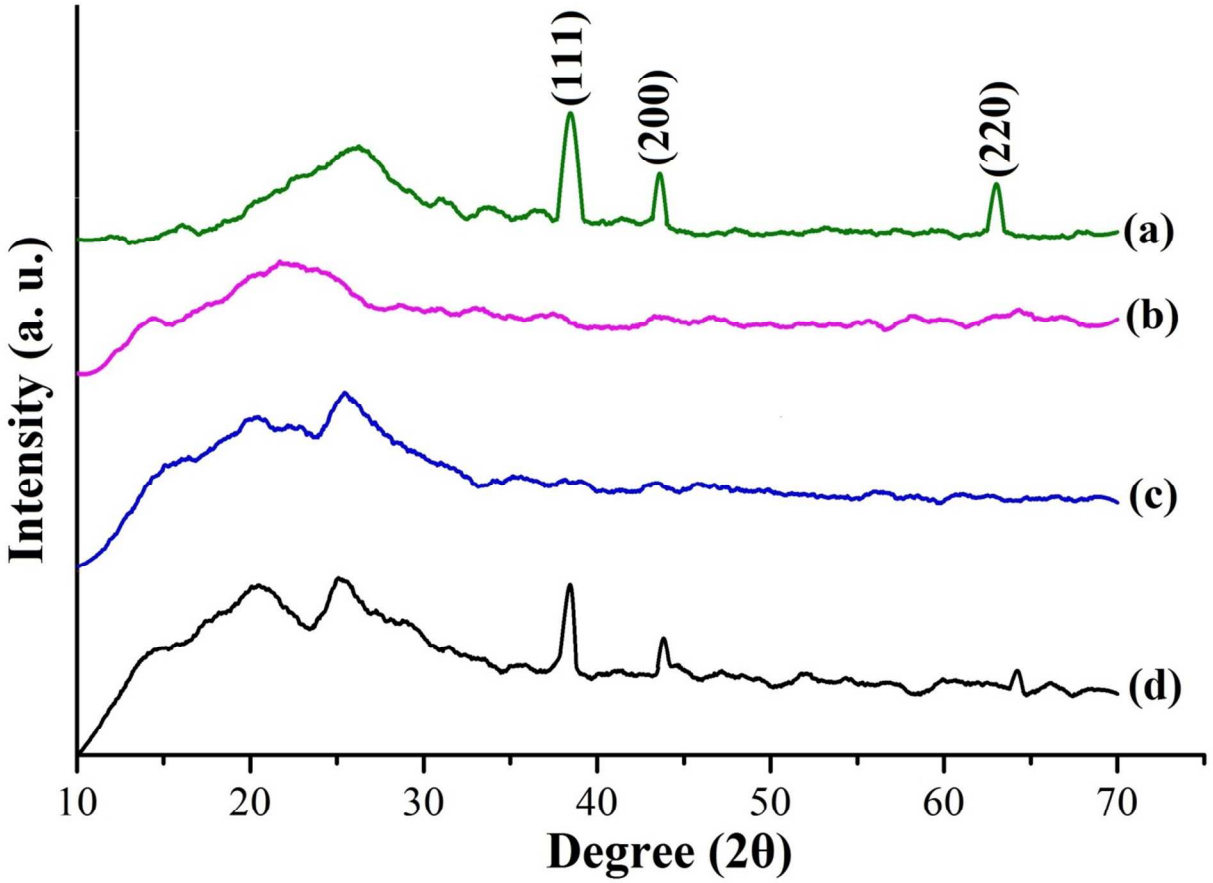

Fig. 3 XRD patterns of (a) Ag nanoparticles, (b) SiO_2 nanoparticles, (c) PAni, (d) SiO_2/PAni-Ag core-shell nanocomposites.

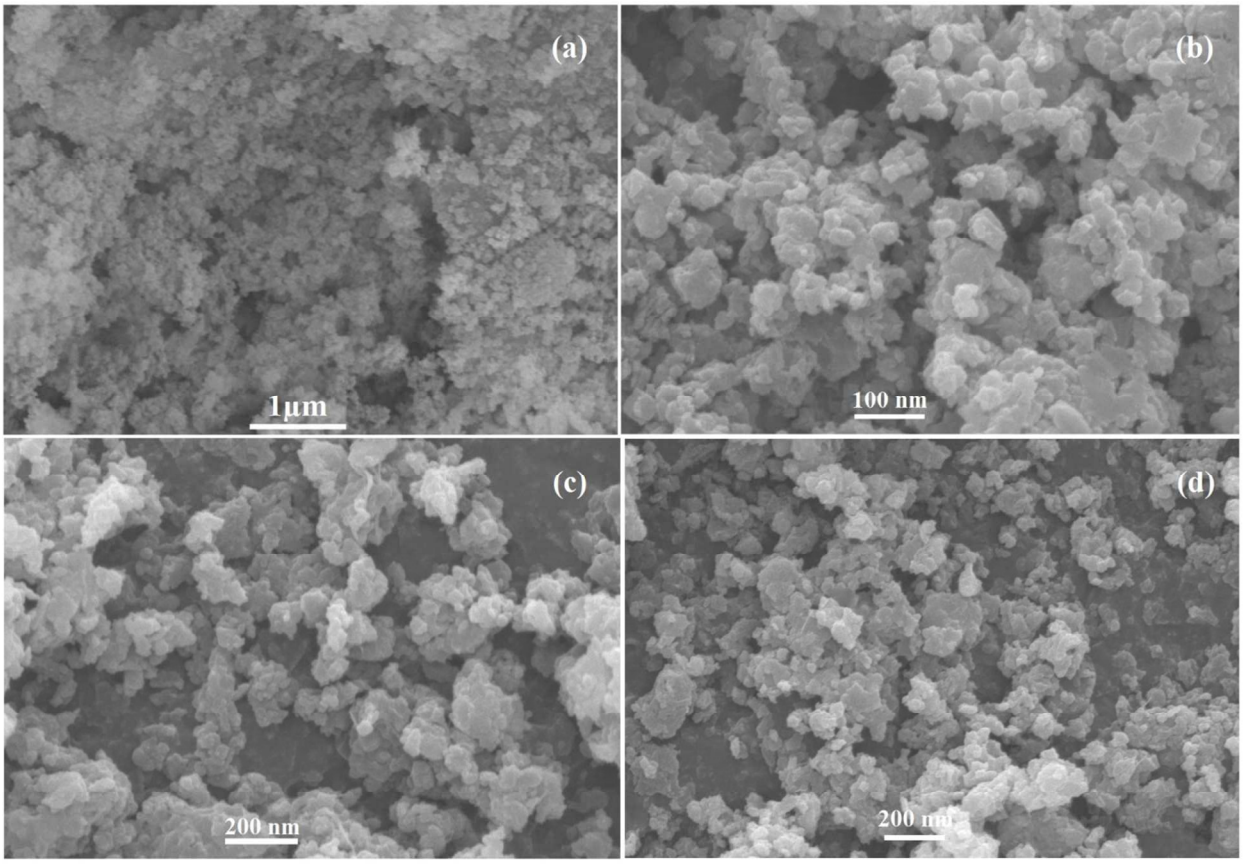

Fig. 4 SEM image of (a) SiO_2 nanoparticles, (b) PAni, (c) SiO_2/PAni core-shell nanocomposites, (d) SiO_2/PAni-Ag nanocomposites.

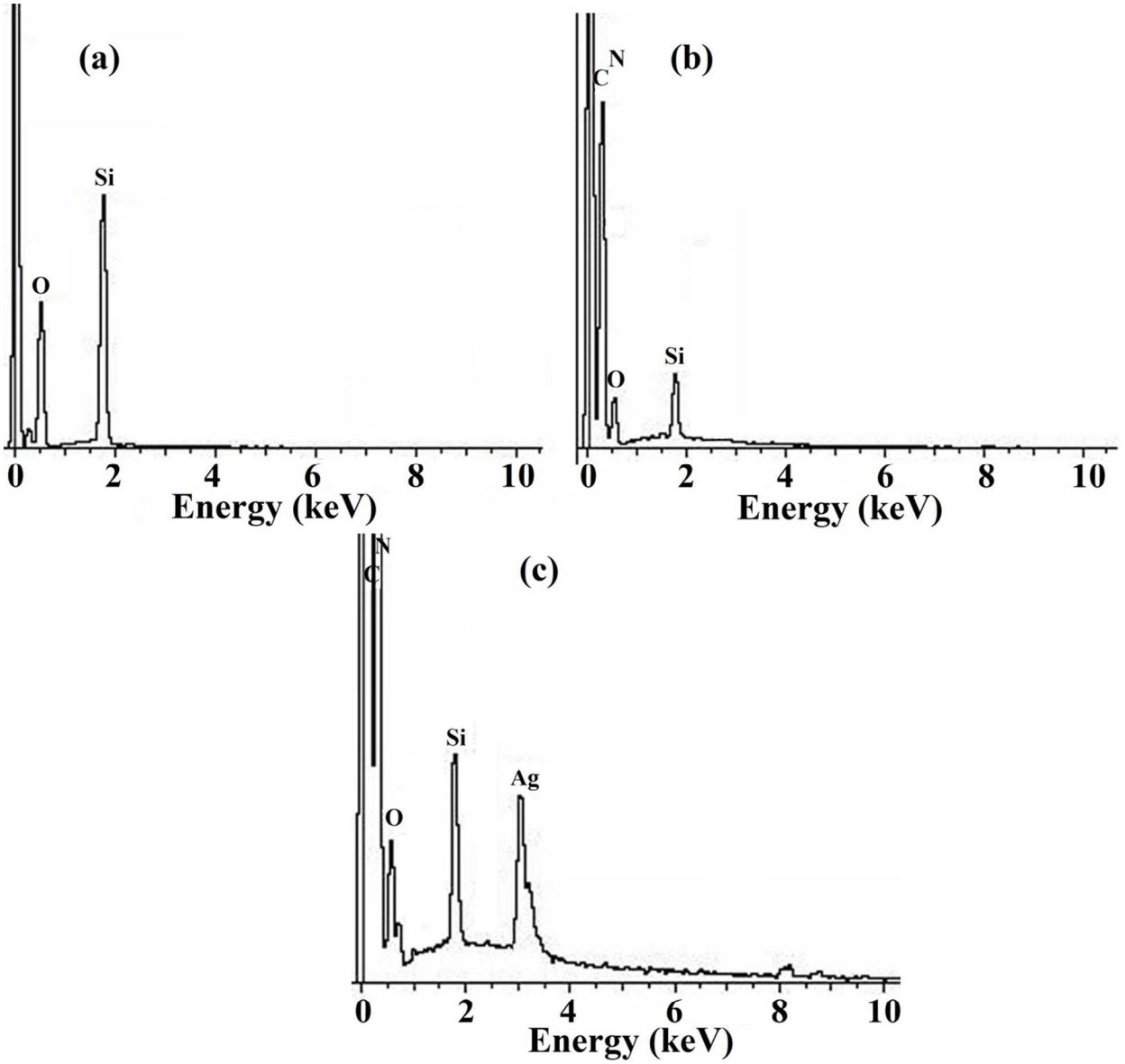

403

404 **Fig. 5** EDX image of (a) SiO_2, (b) SiO_2/PAni core-shell and (b) SiO_2/PAni-Ag core-shell

405 nanocomposites.

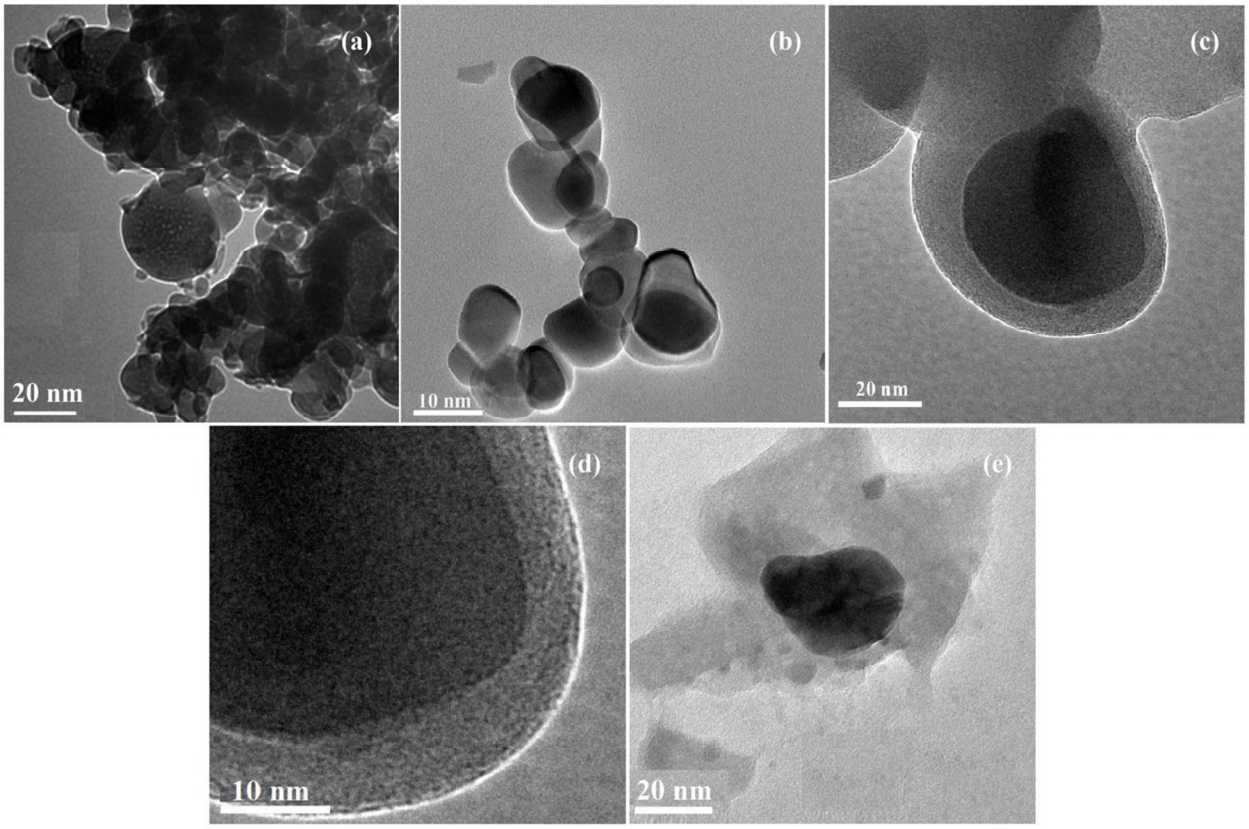

406

407 **Fig. 6** TEM images of (a) SiO_2 nanoparticles, (b) Ag nanoparticles, (c) SiO_2-PAni core-

408 shell nanocomposites, (d) SiO_2-PAni core-shell nanocomposites at higher magnification,

409 (e) SiO_2/PAni-Ag core-shell nanocomposites.

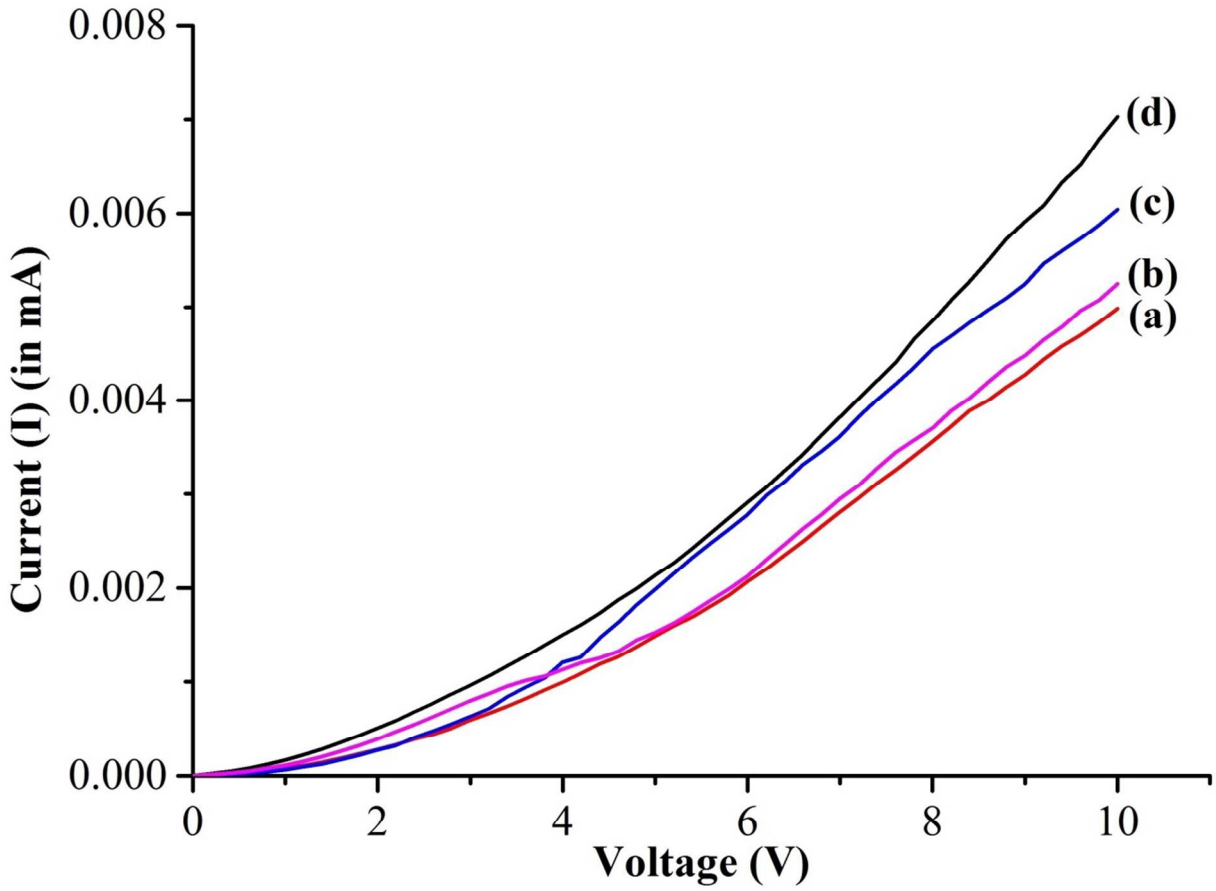

410

411 **Fig. 7** The current-voltage relationships for (a) PAni, (b) SiO_2/PAni-Ag (3%), (c)

412 SiO_2/PAni-Ag (5%), (d) SiO_2/PAni-Ag (7%).

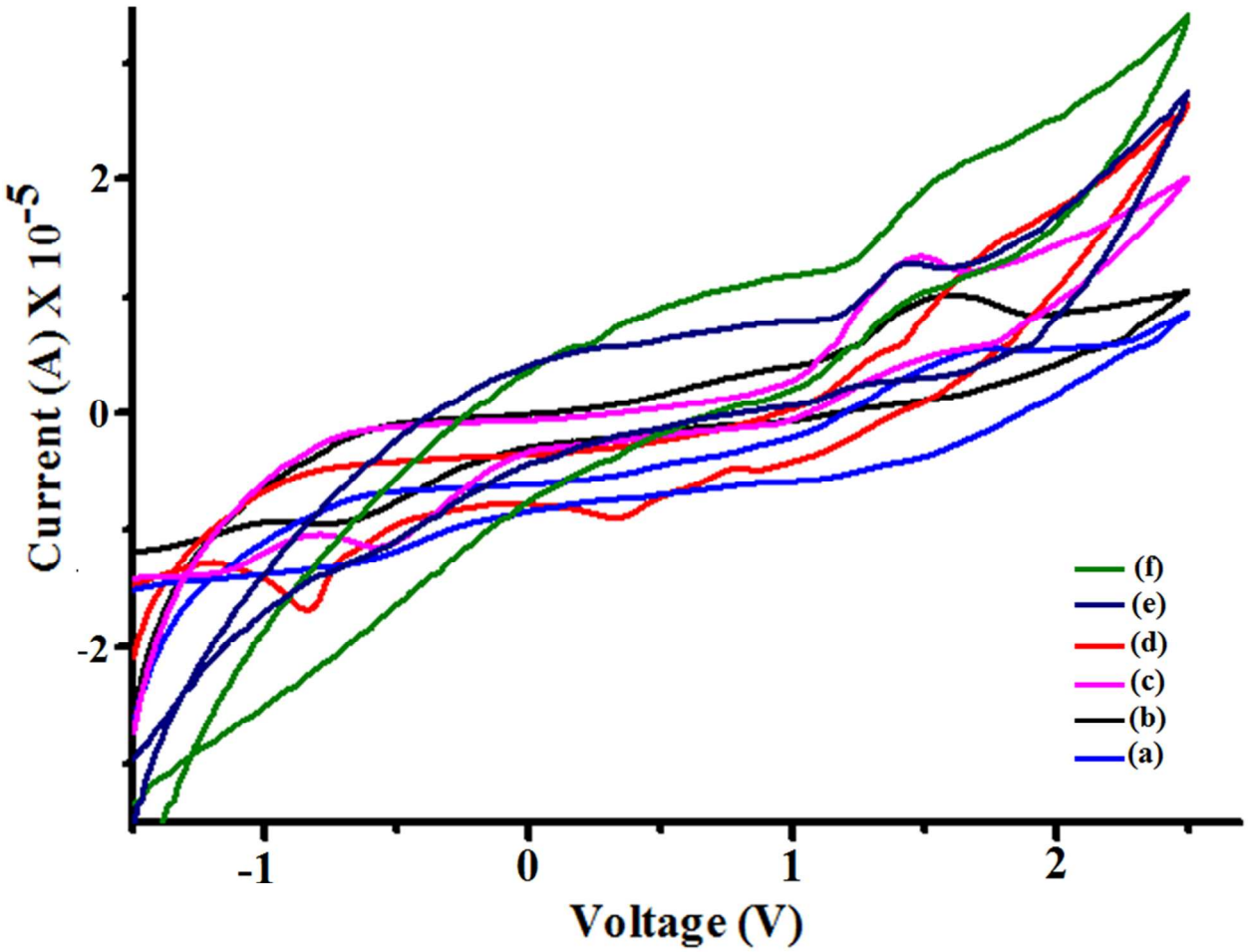

413

414 **Fig. 8** C-V graphs of (a) PAni, (b) SiO_2/PAni (1%) (c) SiO_2/PAni (3%), (d) SiO_2/PAni

415 (5%), (e) SiO_2/PAni (7%), (f) SiO_2/PAni (10%) core-shell nanocomposites.

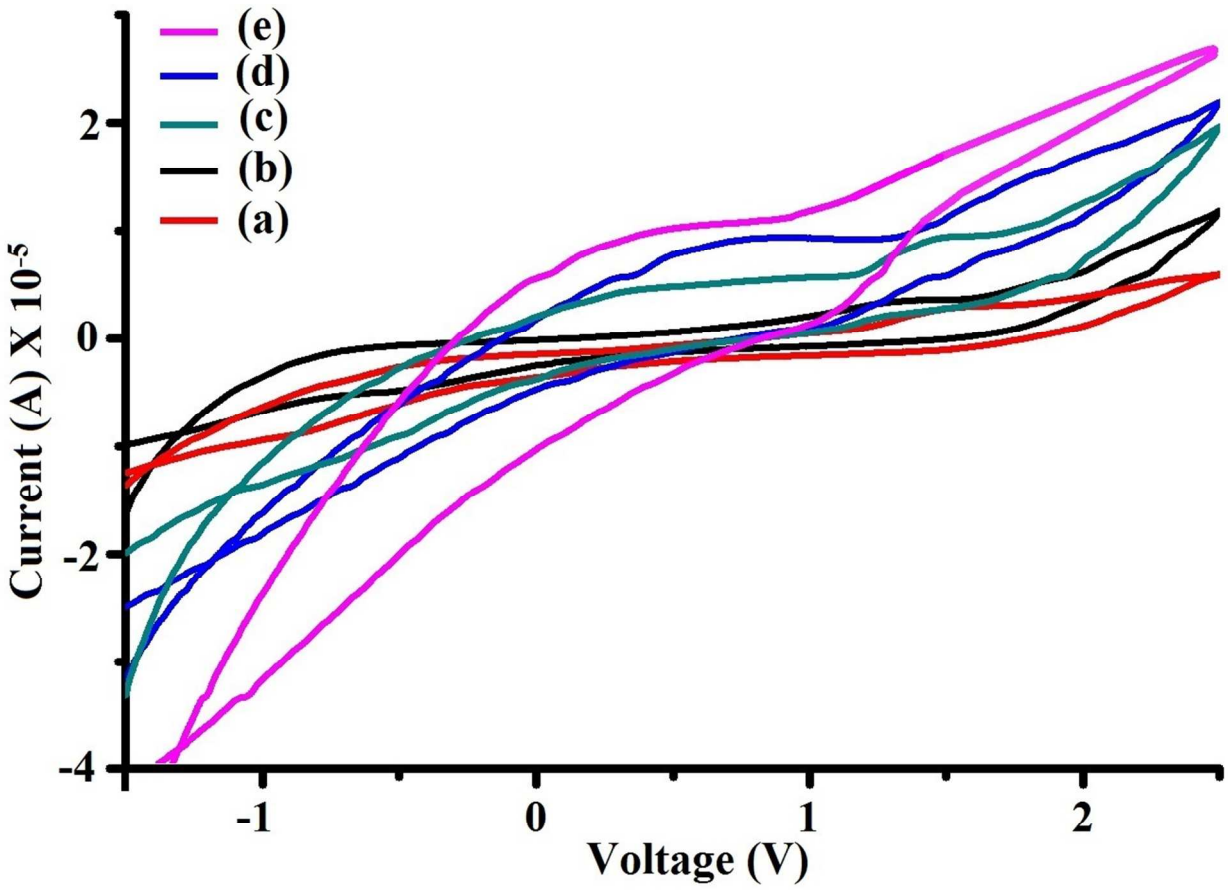

Fig. 9 C-V graphs of (a) SiO_2/PAni-Ag (1%) (b) SiO_2/PAni-Ag (3%), (c) SiO_2/PAni-Ag (5%), (d) SiO_2/PAni-Ag (7%), (e) SiO_2/PAni-Ag (10%) core-shell nanocomposites.

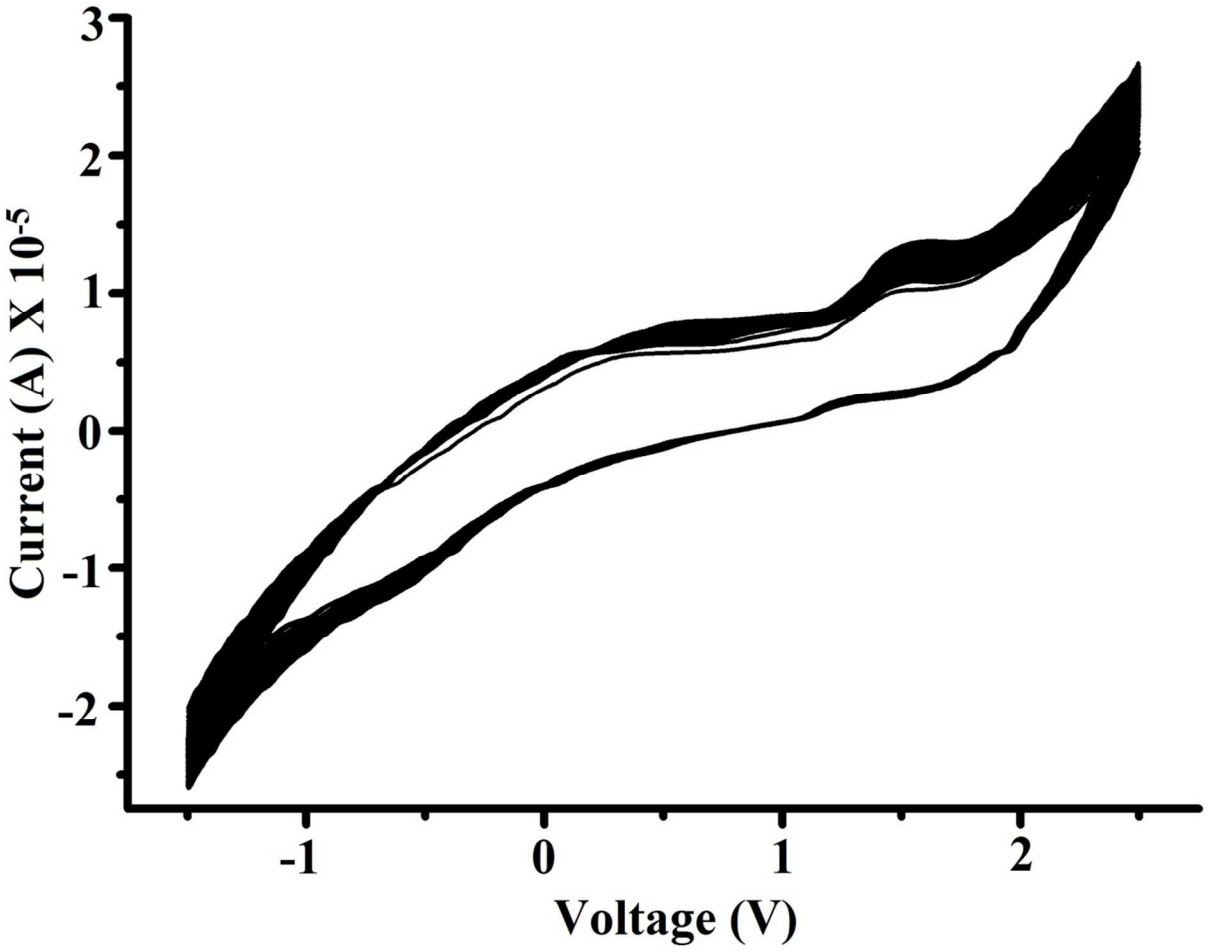

Fig. 10 C-V analysis of SiO_2/PAni-Ag core-shell nanocomposites upto 100 repeated cycles.

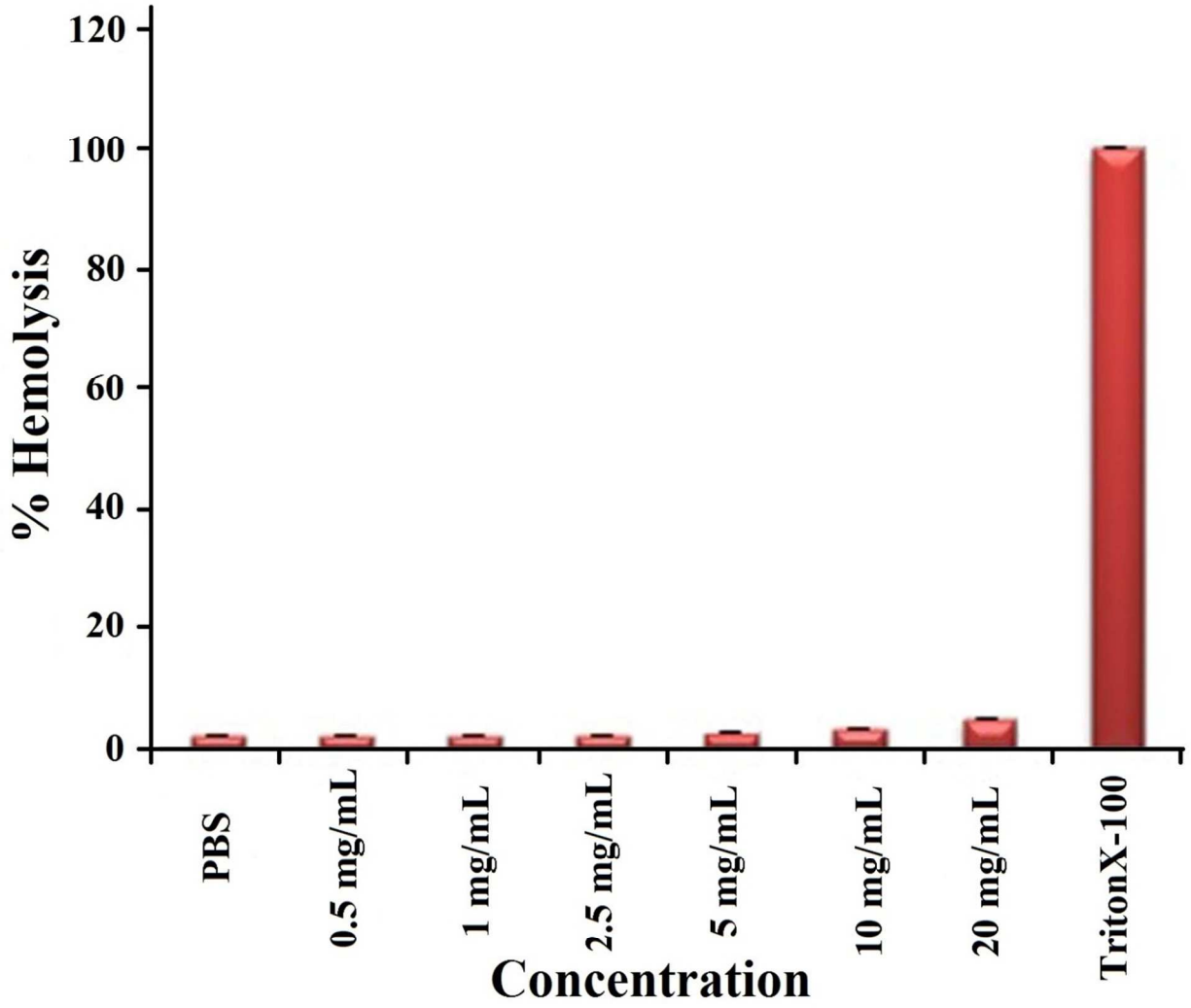

Fig. 11 Haemolytic activity of SiO_2/PAni-Ag core-shell nanocomposites.

Table 1. Electrochemical data of the PAni and SiO_2/PAni nanocomposites, E_{HOMO} and E_{LUMO} signify the highest occupied molecular orbital (HOMO) energy level and lowest unoccupied molecular orbital (LUMO) energy level respectively for the PAni and SiO_2/PAni nanocomposites.

Sample	$\varphi^{ox}_{onset}/E_{HOMO}$	$\varphi^{red}_{onset}/E_{LUMO}$	E_g^{eV} (eV)
PAni	1.62/-6.33	-0.38/–4.32	2.01
SiO_2/PAni			
1%	1.11/-5.82	-0.81/-3.90	1.92
3%	1.14/-5.85	-0.36/-4.35	1.50
5%	0.94/-5.65	-0.49/-4.22	1.43
7%	1.22/-5.93	-0.11/-4.6	1.33
10%	1.30/-6.01	-0.02/-4.73	1.32

[a] onset oxidation potential

[b] onset reduction potential

[c] electrochemical band gap

Table 2. Electrochemical data of SiO_2/PAni-Ag nanocomposites, E_{HOMO} and E_{LUMO} signify the highest occupied molecular orbital (HOMO) energy level and lowest unoccupied molecular orbital (LUMO) energy level respectively for SiO_2/PAni nanocomposites.

Sample	$\varphi^{ox}{}_{onset}/E_{HOMO}$	$\varphi^{red}{}_{onset}/E_{LUMO}$	$E_g{}^{eV}$ (eV)
SiO_2/PAni-Ag			
1%	1.76/-6.47	-0.12/-4.59	1.88
3%	1.76/–6.47	0.29/-4.99	1.47
5%	1.20/-5.91	-0.19/-4.90	1.43
7%	1.16/–5.87	–0.14/–4.57	1.30
10%	1.35/-6.06	–0.09/–4.80	1.26

[a] onset oxidation potential

[b] onset reduction potential

[c] electrochemical band gap

463 **Table 3.** DC-electrical conductivity of PAni, SiO_2/PAni and SiO_2/PAni-Ag nanocomposites with

464 varying the amount of SiO_2, Ag content.

Core-shell nanocomposites	SiO_2-content (%)	Resistivity, ρ (Ωcm) ($X10^3$)	Conductivity, σ (Scm^{-1}) (X 10^{-3})
PAni	0	6.61	0.15
SiO_2/PAni	1	2.06	0.48
SiO_2/PAni-Ag	1	0.89	1.12
SiO_2/PAni	3	0.51	1.96
SiO_2/PAni-Ag	3	0.44	2.27
SiO_2/PAni	5	0.49	2.04
SiO_2/PAni-Ag	5	0.43	2.32
SiO_2/PAni	7	0.24	4.16
SiO_2/PAni-Ag	7	0.19	5.26
SiO_2/PAni	10	0.21	4.76
SiO_2/PAni-Ag	10	0.17	5.88

465